INVESTIGATION OF THE FALSE BOTTOM EFFECTS ON SHIP MODEL TESTS

Mingxin Li, University of Strathclyde, UK
Zhiming Yuan, University of Strathclyde, UK
Guillaume Delefortrie, Ghent University, Belgium

Ship manoeuvring in shallow waters is more difficult and hazardous. In order to estimate the manoeuvring characteristics of the ship in finite water depth, the most effective and reliable method is to carry out the experiments in a shallow water towing tank. Generally, the ship model tests in limited water depth are achieved by varying the water depth in the towing tank. For large size towing tanks, primarily aiming at deep water manoeuvring , such as the 300m×18m×6m tank at the Hamburg Shipbuilding Research Institute (HSVA) , changing the water depth can be achieved either by the installation of an artificial bottom or draining the water out of the towing tank, which is time-consuming and inefficient. In order to improve the efficiency of ship model tests in shallow water, many towing tanks are equipped with the false bottom devices. Thus, varying the water depth can be achieved by adjusting the false bottom. However, a large full-size false bottom is usually accompanied with a small stiffness and will be easily deformed. Therefore, during shallow water tests, the false bottom is usually truncated at a limited size. This leads to the question on how much error could be introduced on the ship behaviour by differences in size and configuration of the false bottom. To the authors' best knowledge, there is limited research that could quantify the error caused by a false bottom with limited horizontal dimensions. The objective of the present study is to investigate the interaction effects between the false bottom and the ship model, and to quantify the test errors (in percentage) due to different configurations and sizes of the false bottom. In order to achieve this, a 3-D Rankine source method based on the potential flow theory with linear free-surface condition is used to investigate the hydrodynamic interaction between the ship model and the false bottom. A contour of errors (in percentage) induced by the limited size of the false bottom was obtained, indicating the effects of the width and submerged depth of the false bottom.

1. INTRODUCTION

It has already been pointed out that ships are most likely to manoeuvre in shallow water, which probably results in larger hydrodynamic forces, control loss and more energy consumption (Sun et al., 2013). It is therefore crucial to investigate the behaviour of a ship in such conditions. The most reliable option is the execution of full-scale experiments, but this is rarely performed due to the massive cost involved.

It has already been pointed out that ships are most likely to manoeuvre in shallow water, which probably results in larger hydrodynamic forces, control loss and more energy consumption [1]. It is therefore crucial to investigate the behaviour of a ship in such conditions. The most reliable option is the execution of full-scale experiments, but this is rarely performed due to the massive cost involved.

As an alternative, the behaviour of a ship in shallow water can be studied theoretically, as was done by Tuck (1966), who used the slender-body theory to solve the disturbance to a stream of shallow water due to a slender body. The slender –body theory was also use by Chen (1995) to investigate the hydrodynamic performance of a ship moving at a near-critical speed in a channel, and by Gourlay to predict the ship squat (Gourlay, 2008).

With the development of higher performance computation, numerical methods have been implemented to solve the problem of a ship moving in shallow water. Numerous examples can be found in literature, such as Saha et al. (2004), who used aRANS method to improve the hull form in shallow water. Terziev et al. (2018) studied the hydrodynamic interaction between the hull and the seabed, the sinkage, trim and resistance of the Duisburg Test Case (DTC) container ship is simulated using CFD, and the results obtained have been compared with the computation by the slender-body theory and various empirical methods. Full numerical simulations are nowadays also possible as shown by Carrica et al. (2016), who studied experimentally and numerically the 20/5 zigzag maneuver for the container ship KCS in shallow water.

Apart from theoretical methods Kijima et al. (1990), among others, proposed a prediction method for ship manoeuvrability in deep and shallow waters, based on approximate formulae, at the initial stage of design. Such empirical formulae can be obtained by analysing existing data or by studying model test results. The latter is still one of the most common methods for estimating ship manoeuvrability to simulate the manoeuvring motion. During such program, multiple experiments are needed to fully capture the hydrodynamic performance. Some examples for the KCS hull model in shallow water were conducted in the towing tank (Carrica et al., 2016; Enger et al., 2010).

The organizing committee of SIMMAN 2014 (Simman, 2014) has a purpose to benchmark the capabilities of different methods for simulating ship manoeuvring (Shen et al., 2014; Yasukawa and Yoshimura, 2015). Since 2014, shallow water tests are also included. During such experiments, the water depth has to be adapted. This means that the water has to be drained out of the tank, which is not always feasible, or at least time consuming. As an alternative some towing tanks are equipped with an artificial bottom. This enables the facility to adjust the water level in a fast way. Examples of such test campaigns can be found in (Mucha et al., 2016; Yeo et al., 2016).

A false bottom facility has also been built at the Maritime and Ocean Engineering Research Institute (MOERI) /KRISO towing tank. With this new facility, the versatile range of research covers the whole field of the naval architecture and ocean engineering. The tank tests are usually conducted by steadily towing the ship model, either in deep water or in shallow water. Considering the full dimension of the tank, the false bottom usually does not cover the full length and width of the tank. The question arises: does the truncated false bottom bring uncertainties when comparing with the full-size real bottom? To the authors' knowledge, this question has never been addressed. One can imagine that such false bottom has an influence on the ship's behaviour, similarly as tank walls can affect the result of a resistance test as described by Raven (2018).

The objective of the present study is to investigate the interaction effects between the false bottom and ship model, and to quantify the test errors (in percentage) due to different configurations and sizes of the false bottom. In this paper, a 3D panel method based on the Rankine type Green function will be used to solve the hydrodynamic problem of a ship model manoeuvring in tanks equipped with various false bottom configurations. This panel method based on the potential flow theory has been widely and successfully applied on various hydrodynamic problems (Yuan et al., 2015; Yuan et al., 2019).

In this paper, the numerical convergence analysis and validation tests were firstly carried out to examine the hydrodynamic forces and wave profiles of a benchmark ship model. After the validations, the present numerical approach was then applied to investigate the false bottom problem. A contour of errors (in percentage) induced by the limited size of the false bottom was finally obtained, showing the effects of the width and submerged depth of the false bottom.

2. Facilities and Methodology

2.1. Numerical towing tank and false bottom facilities

A false bottom was set up symmetrical on the longitudinal centre line of the towing tank. The ship model is towed along the longitudinal centre line. Thus, the lateral forces (moments) are negligible due to the cancellation effect. **Error! Reference source not found.** (a) and (b) are the side view and front view of the towing tank respectively, showing the dimension and position of the false bottom facility. The physical characteristics of the numerical towing tank and false bottom is shown in Table 1. For a ship with forward speed, two right-handed coordinate systems are used: a global reference frame O-$x_0y_0z_0$ fixed to the earth, and a local reference frame o-xyz fixed to the body. Both frames have a positive x-direction pointing towards the bow, positive z direction pointing upwards. The local body-fixed o-xyz, as shown in **Error! Reference source not found.**, is set on the undisturbed free-surface.

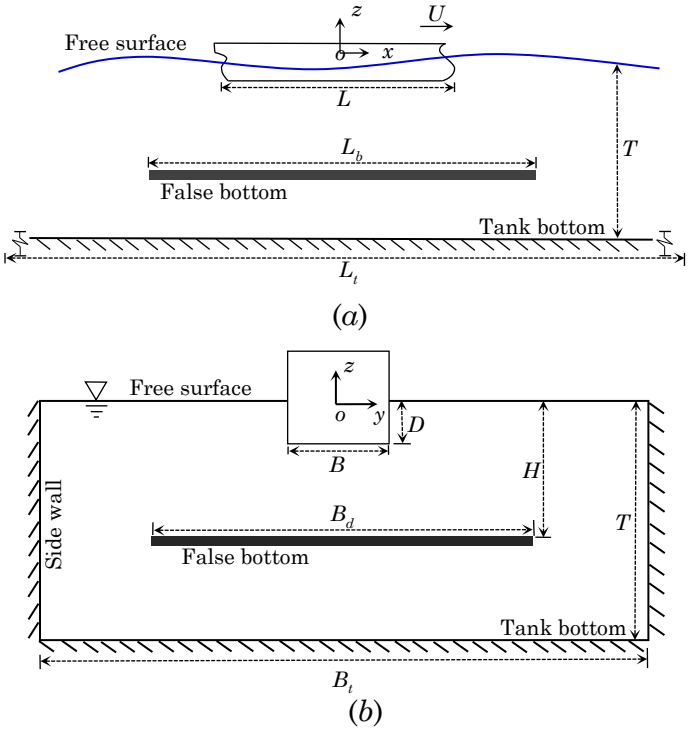

Fig. 1. (a) Side view of the false bottom; the false bottom shows in the figure as a black plane and L denotes the length of the ship hull. (b) Front view of the false bottom. B and D denote the ship's breadth and draught. The breadth of the false bottom and the tank bottom is Bd and Bt, respectively. The false bottom is placed at a submerged depth H. The water depth of the tank is denoted by T.

The sketch of the tank equipped with a false bottom facility is shown in **Error! Reference source not found.**. The dimension of the KRISO towing tank is 200m×16m×7m (L_t×B_t×T). The length of the false bottom L_b is 54m, which is assumed to be sufficiently long and the false bottom effect in the length dimension will not be investigated in this paper. We mainly focus on the truncated effects in breadth dimension. In the present study, the breadth of the false bottom varies from 0 to 16m. The false bottom effect is also determined by the bottom depth H and towing speed U.

Table 1. Characteristics of Numerical towing tank and false-bottom

	Items	Value
Towing tank	Length (m)	200
	Breadth (m)	16
	Depth (m)	7
False-bottom	Length (m)	54
	Breadth (m)	0-16

2.1. Numerical towing tank and false bottom facilities

The present study aims to investigate the interaction effects between the false bottom and the ship model, and to quantify the test errors (in percentage) due to different configurations and sizes of the false bottom. To achieve this goal, a criterion must be identified to quantify the false bottom effects. In captive model tests when a ship is towed along the centre line of a tank with/without false bottom, the differences are mainly represented by the model's hydrodynamic characteristics, including the forces/moments in surge, heave and pitch directions, and the free-surface waves. In this paper, we mainly focus on force-based criteria to assess the difference due to the presence of the false bottom. In particular, the wave-making resistance is used as the quality to calculate the errors (in percentage) due to different configurations and sizes of the false bottom. Of course, the results of sinkage and trim can also be provided as supplementary criteria to show whether the false bottom effects are sensitive to criteria selection. To calculate these quantities (forces/moments/waves), a mathematical model, which is the boundary value problem (BVP), needs to be established. The boundary element method (BEM) based on potential flow theory will be used in this paper to calculate these qualities. Based on the assumptions for the potential flow theory, it neglects the viscosity and compressibility of the flow. Therefore, the fluid domain can be described by using a disturbance velocity potential φ, which represents by the presence of the ship in the fluid domain. In the fluid domain, the potential φ satisfies the Laplace equation:

$$\frac{\partial^2 \varphi}{\partial x^2} + \frac{\partial^2 \varphi}{\partial y^2} + \frac{\partial^2 \varphi}{\partial z^2} = 0 \tag{1}$$

In the body-fixed frame, the kinematic boundary condition on free-surface can be expressed as

$$U\frac{\partial \varphi}{\partial x} + \frac{1}{2}\left[\left(\frac{\partial^2 \varphi}{\partial x^2}\right) + \left(\frac{\partial^2 \varphi}{\partial y^2}\right) + \left(\frac{\partial^2 \varphi}{\partial z^2}\right)\right] = 0 \tag{2}$$

The dynamic boundary condition on the free-surface is

$$U\frac{\partial \zeta}{\partial x} - \frac{\partial \varphi}{\partial z} + \frac{\partial \varphi}{\partial x}\frac{\partial \zeta}{\partial x} + \frac{\partial \varphi}{\partial y}\frac{\partial \zeta}{\partial x} = 0 \tag{3}$$

where $\zeta(x, y, t)$ is the free-surface wave elevation. By applying a Taylor series expanded about $z_0 = 0$ and assuming the disturbance of the fluid is small, the non-linear terms may be neglected when substituting Equation **Error! Reference source not found.** into Equation **Error! Reference source not found.**. In the steady study, it can be simplified to the well-known linearized steady Neumann-Kelvin free-surface condition (Newman, 1977), which can be written as

$$U^2 \frac{\partial^2 \varphi}{\partial x^2} + g \frac{\partial \varphi}{\partial z} = 0 \tag{4}$$

where g is the acceleration due to gravity. Apart from the free-surface condition, there should be no flow through the wetted surface S_B, which is the body surface boundary condition:

$$\frac{\partial \varphi}{\partial n} = U n_1 \tag{5}$$

where $\boldsymbol{n} = (n_1, n_2, n_3)$ is the unit normal vector inward on the wetted body surface. By the same reasoning, the boundary condition on the sea bottom and false bottom can be expressed as

$$\frac{\partial \varphi}{\partial n} = 0 \tag{6}$$

Besides, a radiation condition is imposed on the control surface to ensure that waves vanish at upstream infinity:

$$\varphi \to 0, \ \ \zeta \to 0 \ \ as \ \sqrt{x^2 + y^2} \to \infty \tag{7}$$

Equation (4) to (6) form a completed set of BVP. Each set of BVP is independent and can be solved by the Rankine source panel. Once the unknown potential φ is solved, the pressure over the body-surface can be obtained from linearized Bernoulli's equation

$$p = -\rho U \frac{\partial \varphi}{\partial x} \tag{8}$$

By integrating the pressure over the hull surface, the forces (or moments) can be obtained by

$$F_i = \iint_S p n_i ds \ , \ i = 1, 2, \ldots, 6 \tag{9}$$

where i represents the force in surge, sway, heave, roll, pitch and yaw directions. The wave elevation on the free-surface can be obtained from the dynamic free-surface boundary condition in Equation (3) in the form

$$\zeta(x, y) = \frac{U}{g} \frac{\partial \varphi}{\partial x} \tag{10}$$

2.3. Numerical implementation

To solve the BVP, the in-house-developed numerical program MHydro will be used. In numerical calculations, one cannot consider an infinite free-surface domain. Thus, the computational domain needs to be truncated at a distance away from the ship hull in order to eliminate the wave reflection from the truncated boundaries and to improve the numerical stability in the computational domain. In the present study, a 2nd-order upwind difference scheme is applied on the free-surface to obtain the spatial derivatives of the velocity potential:

$$\frac{\partial^2 \varphi}{\partial x^2}(x_i) = \frac{1}{\Delta x^2}\left(\frac{1}{4}\varphi(x_{i+4}) - 2\varphi(x_{i+3}) + \frac{11}{2}\varphi(x_{i+2}) - 6\varphi(x_{i+1}) + \frac{9}{4}\varphi(x_i)\right) \tag{11}$$

where *i* denotes the element's number related to the collected point, which is influenced by four elements backwards in stream along the x direction. Besides, Equation (7) can be satisfied consequently by applying the Equation (11) (Bunnik, 1999).

3. RESULTS AND DISCUSSIONS OF STEADY PROBLEM

3.1. Validations of Wigley hull

In the present study, we use a benchmark model Wigley III hull in the case studies. In the numerical modelling, the panels are not only distributed on the free-surface and wetted body surface of the ship hull, but also on the false bottom. The mesh of the computational domain is shown in **Error! Reference source not found.**. In the presented study, due to the symmetrical characteristic of the domain, only half of the computation domain is modelled. It allows a reduction of the total number of the panels required in the solution, hence saving computation time. The main particulars of a model scale Wigley III hull are listed in Table 2.

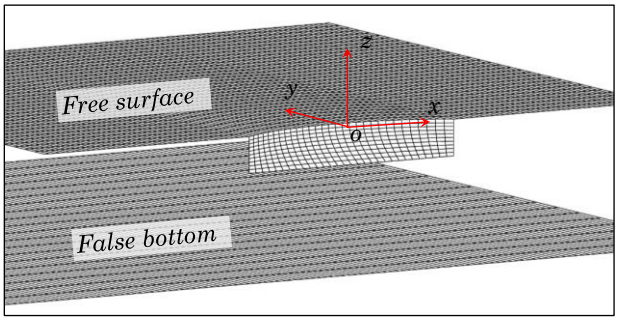

Fig. 2. Panel distribution on the computation domain of a Wigley III model advancing in a tank equipped with a false bottom. There are in total 7354 panels distributed on the total computation domain in this simulation: 4,654 panels distributed on the free-surface S_F, 300 on the wetted body surface S_H and 2400 on the false bottom S_B. The computational domain is truncated at 1.2 L upstream, 1L sideways and 2L downstream.

Table 2. Principal dimensions of the Wigley III model

Dimensions Item	Value
Length (m)	3.0
Breadth (m)	0.3
Draft (m)	0.1875

To validate the present methodology and numerical method, we calculated the wave-making resistance coefficients C_w and wave profile ζ at the starboard of the ship model. The non-dimensional wave-making resistance coefficient C_w, is defined as:

$$C_w = \frac{R_w}{(1/2)\rho U^2 S} \tag{12}$$

where S is the area of the wet body surface and R_w denotes the wave-making resistance, which equals to F_1 in Equation (9). The numerical results of the wave resistance coefficient and wave elevation are obtained and compared with the experimental results from different institutions (Kajitani et al., 1983) as well as the numerical results from Huang et al. (2013) obtained from Neumann-Michell theory, as shown in Fig. 3 (*a*) and (*b*), respectively. The results show that a satisfactory agreement is achieved between the numerical predictions and experimental measurements. The waves at both the bow and stern areas are underestimated due to the linear assumption of the present method. The non-linear effect cannot be estimated by using the present linear method.

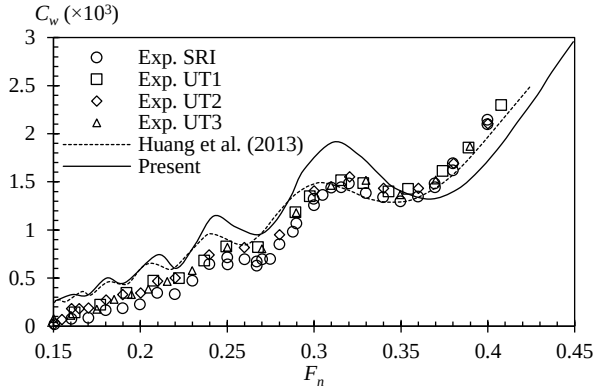

(*a*)

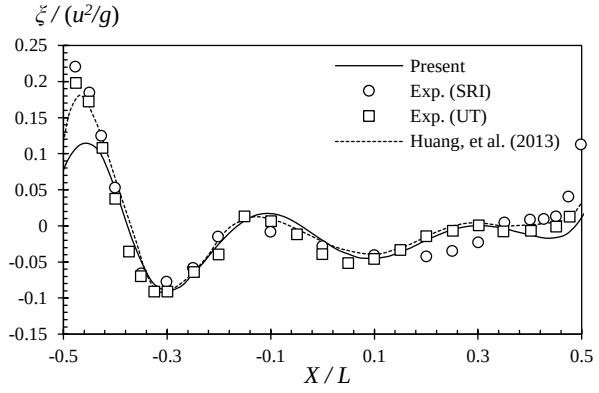

(*b*)

Fig. 3. Validations of the present results. (a) Wave-making resistance coefficient C_w*; (b) Wave profile along the Wigley Ш hull at* $F_n = 0.25$.

3.2. Effect of B_d and H

In this section, only the steady effects of false-bottom are discussed. It indicates that the false-bottom covers the full length of the tank. Based on this assumption, the BVP can be treated as a steady problem, and all the quantities, including the velocity potential and the pressure, are time-independent. The parameters which determine the false-bottom effect will include the breadth B_d (or non-dimensional breadth B_d/B_t) and submerged depth H (or non-dimensional submerged depth H/D) of the false bottom, and the towing speed of the ship model U (or non-dimensional speed $U/\sqrt{gL}$, which is called Froude number F_n). B_d/B_t varies from 0 to 1, in which $B_d/B_t = 0$ indicates the false bottom doesn't exist, and B_d

/B_t =1 indicates the false bottom covers a full breadth of the tank. H/D varies from 1 to infinite, in which H/D =1 indicates the under keel clearance (UKC) is zero, and H/D = *inf*. indicates deep water. The Froude number varies from 0.1 to 0.7, which covers the most common towing speeds. Before quantifying the effect of false-bottom breadth, we have to find the cases that the false bottom with the full-breadth (B_d /B_t =1) as the standard criterion. In the next few sections, the results at B_d /B_t =1 will be used as comparative data base. Fig. 4 shows the calculated wave-making resistance coefficient C_w of a Wigley model moving at different H/D. The results show that the wave-making resistance is heavily affected by the water depth. As the water depth decreases, the amplitude of the wave-making resistance coefficient increases rapidly, and the peaks of C_w shift towards lower Froude numbers. These peaks usually appear at the critical speed range, where the water depth Froude number ($F_h = U/\sqrt{gH}$) approaches 1.

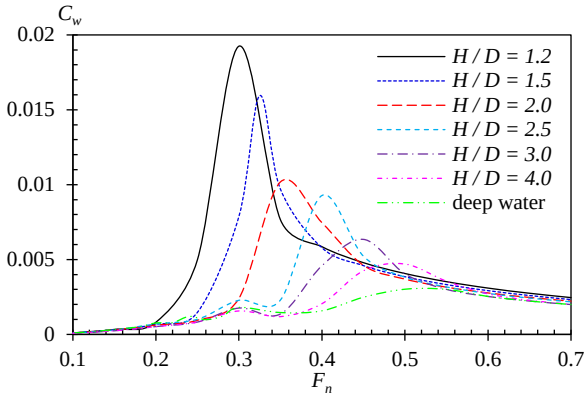

Fig. 4. Comparison of wave-making resistance coefficient C_w at different H/D when the false bottom covers a full tank breadth.

Fig. 5 shows the results of the wave-making resistance coefficient at different false-bottom breadths. Two typical submerged depths are studied here, H/D =4.0 and 10.0, which represent the boundary between deep and shallow water and (infinite) deep water respectively. It can be concluded from Fig. 5 (a) that in infinite deep water (H/D =10.0), the effect of the false bottom's breadth is very limited. The differences are mainly observed at the peak region of C_w curves, with Froude number ranging from 0.5 to 0.7. However, the false-bottom effects are more important at the boundary of shallow water (H/D =4.0). The results in Fig. 5 indicate that, when conducting shallow water tests by using a false bottom facility, the test results are very sensitive to the breadth of the false bottom near the critical speed. It can also be found that the difference of C_w induced by the limited-breadth of the false bottom varies with the towing speed. At low and very high Froude number (F_n <0.4 and F_n >0.8), the test results are less sensitive to the breadth of the false bottom. Special attention should be paid to the shallow water tests in near critical region at 0.8<F_h <1.2, ($F_h = U/\sqrt{gH}$ is the water depth Froude number). The test results are significantly affected by the breadth of the false bottom.

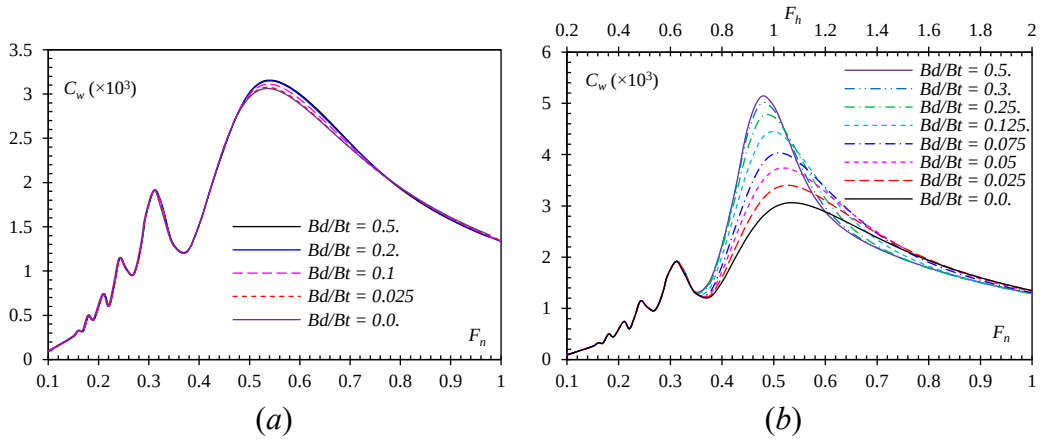

Fig. 5.Comparison of wave-making resistance coefficient at different B_d/B_t. (a) H/D = 10.0; (b) H/D = 4.0.

3.3 False-bottom effect contour

It is clearly shown in Fig. 5 that all of the three parameters (H/D, B_d/B_t and F_n) play an important role when determining the false-bottom effect. In this section, we will investigate the false-bottom effect induced by the combination of all these three parameters. To quantify the test errors (in percentage) induced by the limited breadth of the false bottom, we define a test error coefficient C_{rw} based on the wave-making resistance as following:

$$C_{rw} = \frac{C_w^{B_d/B_t} - C_w^{inf}}{C_w^{inf}} \times 100\% \tag{13}$$

where $C_w^{B_d/B_t}$ is the wave-making resistance coefficient C_w at B_d/B_t, and C_w^{inf} is the wave-making resistance coefficient by using a full-breadth bottom ($B_d/B_t = 1$) in the same water depth as $C_w^{B_d/B_t}$. It has been shown that the shallow water effects become very critical at $H/D < 4$ (Vantorre, 2003). Hence, we consider the effect of the false bottom at depth ranging at $1.2 < H/D < 3.4$. Fig. 5 shows that the difference between the results at $B_d/B_t = 0.3$ and $B_d/B_t = 0.5$ is negligible for most of the Froude numbers. Therefore, the present study only investigates the false bottom effect at $B_d/B_t < 0.35$. Particularly, $B_d/B_t = 0$ indicates the results in a given water depth without false-bottom. Table 3 lists the non-dimensional parameters of all test cases.

Table 3. Test cases of the non-dimensionalised parameters

Test items	Value range
B_d/B_t	0.0-0.35
H/D	1.2-3.4
F_n	0.06-0.4

Fig. 6 presents the 3D contour of the error coefficient C_{rw} as function of the non-dimensional false bottom depth H/D and non-dimensional breadth B_d/B_t. Fig. 6 (*a*) to (*f*) show the results under subcritical speed $F_h < 0.73$ ($F_h = 0.73$ is based on the minimum water depth at $H/D = 1.2$). The false bottom effect is very limited in most of the areas and the test error C_{rw} will not exceed 10% in all test cases. It can be concluded

that when conducting ship model tests at a speed below $F_h < 0.75$, the false-bottom effect is small (<10%). As long as the breadth of the false bottom is larger than 10 times of the ship breadth, the test results by using the false-bottom facility can represent the real shallow water and the deviation will decrease with increasing width of the false bottom. This conclusion is consistent with the wave-making resistance shown in Fig. 6 (*b*) when $F_h < 0.75$.

As F_h gradually approaches the critical speed ($F_h = 1$), as shown in Fig. 6 (*g*)-(*i*), the test error coefficient C_{rw} increases rapidly. At $F_h = 0.91$, as shown in Fig. 6 (g), the maximum error caused by false-bottom effect can reach 80%. However, these errors are mainly concentrated in the lower-left corner where $H/D < 1.8$ and $B_d/B_t < 0.1$. As long as the breadth of the false bottom is larger than 8 times of the ship breadth ($B_d/B > 8$), the false-bottom effect can be neglected.

As F_h becomes larger than critical speed ($F_h > 1$), which for displacement ships is only a theoretical condition, as shown in Fig. 6 (*h*) and (*i*), the false-bottom effect is expanded to cover a larger area. In order to get accurate shallow water test result without false-bottom effect, the breadth of the false bottom should be at least 15 times as that of the ship ($B_d/B > 15$, or $B_d/B_t > 0.25$), It should be noted that there are two sensitive regions in these two figures, presented in red and blue in the contour figure. These two regions (red region is positive and blue region is negative) represent a very large test error induced by the false bottom. It can be explained from the results shown in Fig. 4. It can be found that when the speed of the advancing ship is at the supercritical speed, the wave-making coefficient C_w has a decreasing trend until reaching a constant value. Due to the phase lag of the peaks at different H/D, the values of the C_w at a deeper water may be larger than that in a shallower water at the same speed.

In general the results seem to agree well with the recommendations issued by ITTC in their procedure 7.5-02-06-02 Captive Model Test. The test speed should be limited to 80% of the critical Froude number:

$$F_{h,crit} = \left[2 \sin\left(\frac{\arcsin(1-m)}{3}\right)\right]^{\frac{3}{2}} \tag{14}$$

and the influence width,

$$y_{infl} = 5B(F_h + 1) \tag{15}$$

which represents the lateral reach needed to avoid restricted water effects, seems also to provide a safe limit for the lateral reach of a false bottom, which needs to be larger at larger test speeds and decreasing water depths, hence, at increasing depth Froude numbers.

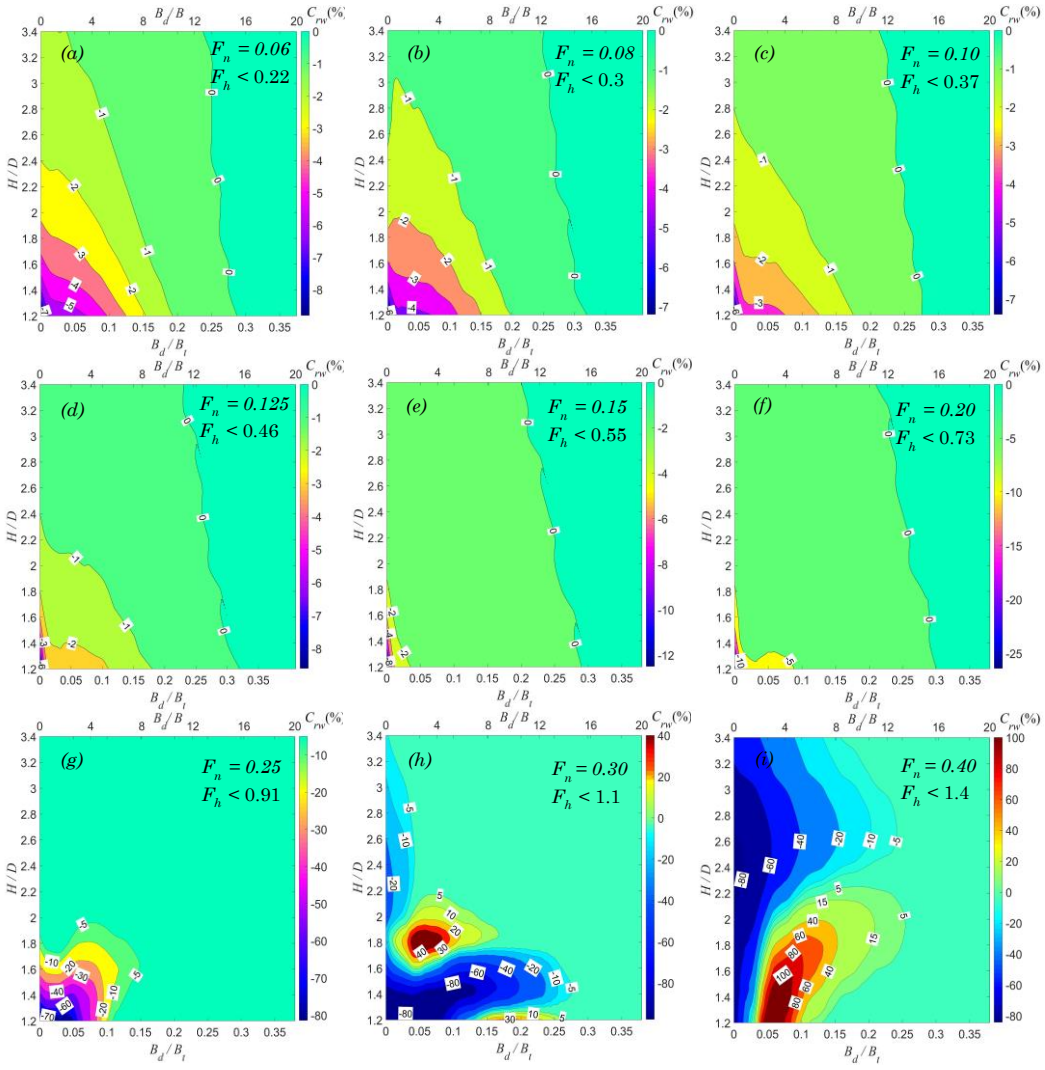

Fig. 6. 3D surface contour of the error coefficient C_{rw} *as function of H/D and* B_d/B_t*. The upper* x*-axis in each figure is the false bottom breadth to ship breadth radio.*

4. DISCUSSIONS OF UNSTEADY PROBLEM

In this section, a preliminary discussion on the unsteady effect of the false bottom will be presented. The term 'unsteady' is used here to describe the time varying process when a ship is moving from deeper water (h_1) to shallower water (h_2) by using a false bottom facility of limited length, as shown in **Error! Reference source not found.**. At each time step, the boundary conditions are different. Therefore, the velocity potential of the fluid domain is time dependent, and it requires an unsteady free-surface condition to account for this unsteady effect.

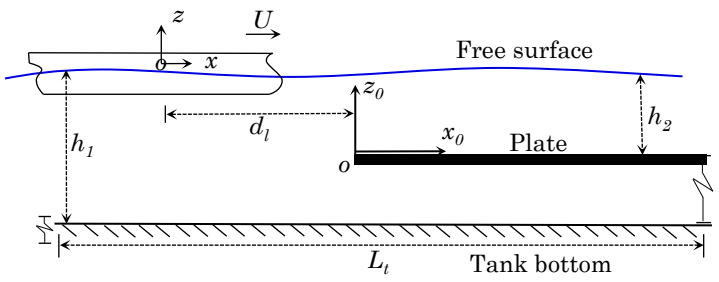

Fig. 7. Side view of the unsteady problem when a ship is moving from deep water to shallow water with false bottom facility.

The unsteady kinematic and dynamic free-surface condition can be written as following

$$\frac{\partial \zeta}{\partial t} - U\frac{\partial \zeta}{\partial x} - \frac{\partial \varphi}{\partial z} = 0 \tag{16}$$

$$\zeta + \frac{1}{g}\frac{\partial \varphi}{\partial t} - \frac{U}{g}\frac{\partial \varphi}{\partial x} = 0 \tag{17}$$

The unsteady pressure can be obtained from linearized Bernoulli's equation

$$p = -\rho\left(\frac{\partial \varphi}{\partial t} - U\frac{\partial \varphi}{\partial x}\right) \tag{18}$$

In addition, the free-surface elevation can be obtained from dynamic free-surface boundary condition

$$\zeta(x, y, t) = -\frac{1}{g}\left(\frac{\partial \varphi}{\partial t} - U\frac{\partial \varphi}{\partial x}\right) \tag{19}$$

To solve this unsteady nonlinear BVP, we developed an implicit finite-difference algorithm. The nonlinear equation (17) can be obtained iteratively. At each time step, the time-independent terms in (16) are obtained explicitly. The dynamic condition in equation (17) is then satisfied through an implicit Euler discretization scheme. The main particulars of a KCS in model scale with a scale factor of 1/31.6 are listed in Table 2.

Table 4. Principal dimensions of the KCS model

Dimensions Item	**Value**
Scale ratio (-)	31.6
Length (m)	7.2786
Breadth (m)	1.019
Draft (m)	0.3418

We calculated the wave-making resistance, heave force and pitch moment in time domain. The non-dimensional heave force coefficient C_Z and pitch moment coefficient C_M, are defined as

$$C_Z = \frac{F_3}{(1/2)\rho U^2 S} \tag{20}$$

$$C_M = \frac{F_5}{(1/2)\rho U^2 SL} \tag{21}$$

Error! Reference source not found. shows the results of the unsteady hydrodynamic forces (or moment) when the ship model is moving from h_1 to h_2. dl/L=0 indicates the moment when the water depth is changing from h_1 to h_2. It is obvious to find that all the hydrodynamic forces experience an impulse near the leading edge of the false bottom. After this impulse, the ship will gradually reach harmonic-like oscillations due to the unsteady effect of the free-surface. Comparing with the constant forces when the model is moving steadily in shallow water with constant depth (as shown in blue curves in each figure), it can be observed that the heave force and pitch moment are more 'unsteady'. Another important finding from this preliminary study is that these impulses do not decay rapidly. The amplitude of the oscillation will retain almost a constant value, even though the ship model has been moving a long distance on the false bottom. This preliminary finding indicates when conducting shallow water tests by using a false-bottom facility, the test results may not be steady, if the ship model is accelerated from deep water. Of course, the ship model can be towed initially on the top of the false bottom. An impulse might still be excited due to the acceleration. In order to get a steady result, the false bottom has to be sufficiently long, so that this impulse can be damped. A further study is required to quantify the effective length of the false bottom, in which the results are not oscillating.

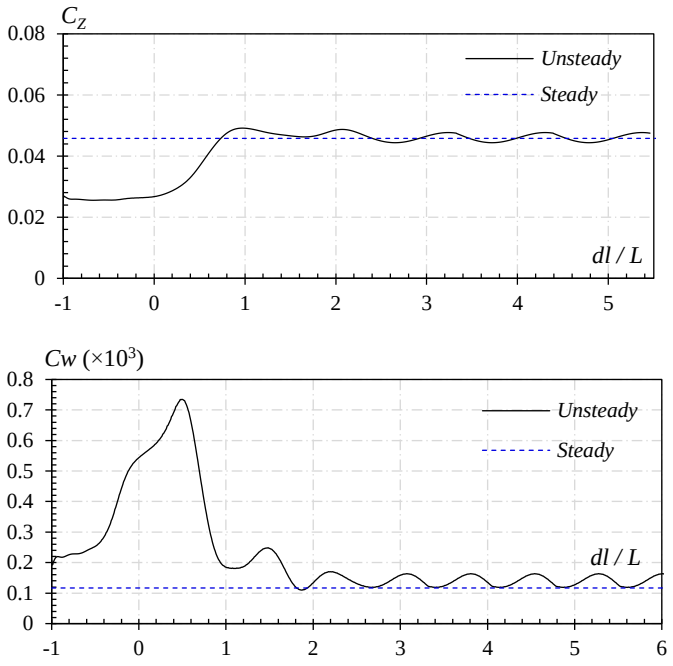

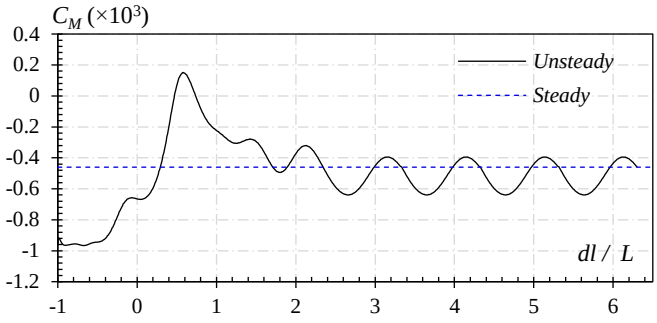

Fig. 8. Unsteady force coefficient of a KCS model moving from h_1 to h_2 at a speed of u = 0.8007 m/s. The depth Froude number Fh_1 = 0.1 and Fh_2 = 0.25. The blue lines are the steady results when the ship is moving above a flat bottom in shallow water.

5. CONCLUSIONS

The false bottom facilities installed in a towing tank can improve the efficiency to measure the hydrodynamic forces of a ship moving in the shallow water. However, our understanding on the configuration and size of the false bottom is limited as concerned, it is important to quantify the false-bottom effect before the false bottoms are widely equipped in towing tanks. In our numerical study, we investigate both the steady and unsteady false-bottom effect. From the numerical calculations, the following conclusions can be drawn:

1) If the false bottom is infinitely long (the same length as the towing tank), the false-bottom effects can be neglected when the breadth of the false bottom is larger than 15 times of the ship breadth (B_d / B > 15). The presently proposed influence width formula by the ITTC, $y_{infl} = 5B(F_h+1)$, proposes a safe estimation of the necessary width of the false bottom and suggests a false bottom breadth of 15 times the ship breadth at F_h = 0.5.
2) If the length of the false bottom is limited, the unsteady false-bottom effect becomes very evident. The measurements may be subject to an oscillation and it may take a long time to decay these oscillations, hence reducing the effective testing length. Such phenomenon is also registered in the horizontal direction when studying ship-bank interaction. It is advisable to check the steadiness of the measured signals in such case.

The present paper focused on the resistance, heave and pitch motion during straight line tests. Additional research is needed to cover manoeuvring motions.

6. Nomenclature

A_w	Water plane area
B	Breadth of the model
B_d	Breadth of the false bottom
B_t	Breadth of the towing tank
C_{rw}	Relative values of the wave-making resistance coefficient
C_w	Wave-making resistance coefficient
D	Draught of the model

d_l	Distance from the ship centre to the boundary of the false bottom
F_n	Froude number of the ship hull
F_r	Depth Froude number for the towing tank
g	acceleration due to gravity
H	Depth of the false bottom
I_w	Second moment of the water plane about the y-axis
L	Length of the model
L_b	Length of the false bottom
L_t	Length of the towing tank
m	Blockage (wetted cross section of the ship ÷ wetted cross section of the tank)
n	Unit normal vector
R_w	Wave-making resistance
S	Surface area of the model
S_B	False bottom surface
S_F	Free-surface
S_H	Hull surface
T	Depth of the towing tank
t	Time domain
U	Uniform velocity in the positive x-direction
ζ	Wave elevation
λ	Wave length
ρ	Density of the water
φ	Disturbed velocity potential due to the presence of the body

7. References

1. Sun, X., et al., *Analysis of the operational energy efficiency for inland river ships.* Transportation Research Part D: Transport and Environment, 2013. **22**: p. 34-39.
2. Tuck, E.O., *Shallow-water flows past slender bodies.* Journal of fluid mechanics, 1966. **26**(1): p. 81-95.
3. Chen, X.-N. and S.D. Sharma, *A slender ship moving at a near-critical speed in a shallow channel.* Journal of Fluid Mechanics, 1995. **291**: p. 263-285.
4. Gourlay, T., *Slender-body methods for predicting ship squat.* Ocean Engineering, 2008. **35**(2): p. 191-200.
5. Saha, G.K., K. Suzuki, and H. Kai, *Hydrodynamic optimization of ship hull forms in shallow water.* Journal of Marine Science and Technology, 2004. **9**(2): p. 51-62.
6. Carrica, P.M., et al., *Direct simulation and experimental study of zigzag maneuver of KCS in shallow water.* Ocean engineering, 2016. **112**: p. 117-133.
7. Kijima, K. and Y. Nakiri, *Prediction method of ship manoeuvrability in deep and shallow waters*, in *Marine Simulation and Ship Manoeuvrability*, C.S.J. Cross, Editor. 1990: Tokyo, Japan. p. p.311.

8. Enger, S., M. Perić, and R. Perić. *Simulation of flow around KCS-hull*. in *Proceedings from Gothenburg 2010—A Workshop on Numerical Ship Hydrodynamics, Gothenburg*. 2010.
9. Simman. *Workshop on Verification and Validation of Ship Manoeuvring Simulation Methods*. in *simman2014.dk*. 2014. Lyngby, Denmark.
10. Shen, Z., D. Wan, and P.M. Carrica. *RANS simulations of free maneuvers with moving rudders and propellers using overset grids in OpenFOAM*. in *SIMMAN workshop on Verification and Validation of Ship Maneuvering Simulation Methods. Presented at the SIMMAN workshop on Verification and Validation of Ship Maneuvering Simulation Methods, Lyngby, Denmark*. 2014.
11. Yasukawa, H. and Y. Yoshimura, *Introduction of MMG standard method for ship maneuvering predictions.* Journal of Marine Science and Technology, 2015. **20**(1): p. 37-52.
12. Mucha, P., et al. *Validation studies on numerical prediction of ship squat and resistance in shallow water*. in *4th MASHCON International Conference on Ship Manoeuvring in Shallow and Confined Water with special focus on Ship Bottom Interaction*. 2016. Elbcampus, Hamburg, Germany.
13. Yeo, D.J., K. Yun, and Y. Kim. *Experimental Study on the Manoeuvrability of KVLCC2 in Shallow Water*. in *4th MASHCO International Conference on Ship Manoeuvring in Shallow and Confined Water with special focus on Ship Bottom Interaction*. 2016. Elbcampus, Hamburg, Germany.
14. Yuan, Z.-M., et al., *Hydrodynamic interactions between two ships travelling or stationary in shallow waters.* Ocean Engineering, 2015. **108**: p. 620-635.
15. Yuan, Z.-M., et al., *Steady hydrodynamic interaction between human swimmers.* Journal of the Royal Society Interface, 2019. **16**(150): p. 20180768.
16. Newman, J.N., *Marine hydrodynamics*. 1977: MIT press.
17. Bunnik, T.H.J., *Seakeeping calculations for ships, taking into account the non-linear steady waves*, in *Ph.D. thesis*. 1999, Delft University of Technology, The Netherlands.
18. Kajitani, H., et al., *The summary of the cooperative experiment on Wigley parabolic model in Japan*. 1983, TOKYO UNIV (JAPAN).
19. Huang, F., C. Yang, and F. Noblesse, *Numerical implementation and validation of the Neumann–Michell theory of ship waves.* European Journal of Mechanics-B/Fluids, 2013. **42**: p. 47-68.
20. Vantorre, M. *Review of practical methods for assessing shallow and restricted water effects*. in *International Conference on Marine Simulation and Ship Maneuverability (MARSIM). Kanazawa, Japan. WS-4-1-WS-4-11*. 2003.